NANO LETTERS

pubs.acs.org/NanoLett Letter

Non-Invasive Nanoscale Potentiometry and Ballistic Transport in Epigraphene Nanoribbons

Alessandro De Cecco, Vladimir S. Prudkovskiy, David Wander, Rini Ganguly, Claire Berger, Walt A. de Heer, Hervé Courtois, and Clemens B. Winkelmann*

Cite This: *Nano Lett.* 2020, 20, 3786–3790 Read Online

ACCESS | Metrics & More | Article Recommendations | Supporting Information

ABSTRACT: The recent observation of non-classical electron transport regimes in two-dimensional materials has called for new high-resolution non-invasive techniques to locally probe electronic properties. We introduce a novel hybrid scanning probe technique to map the local resistance and electrochemical potential with nm- and μV resolution, and we apply it to study epigraphene nanoribbons grown on the sidewalls of SiC substrate steps. Remarkably, the potential drop is non-uniform along the ribbons, and μm-long segments show no potential variation with distance. The potential maps are in excellent agreement with measurements of the local resistance. This reveals ballistic transport, compatible with μm-long room-temperature electronic mean-free paths.

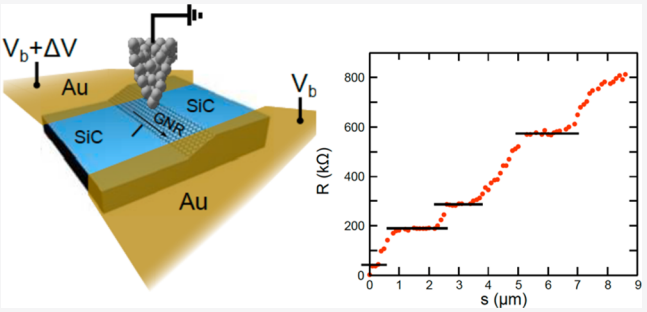

KEYWORDS: *Epigraphene, graphene nanoribbons, ballistic transport, scanning tunneling potentiometry*

Recent experiments have demonstrated that epigraphene nanoribbons grown on the sidewalls of SiC substrate steps[1,2] present one-dimensional ballistic transport properties involving a single quantum channel of conductance with electronic mean-free paths exceeding 10 μm even at room temperature.[3] These confirmed properties[4,5] are in contrast with the Coulomb blockade or disordered-induced insulating behavior observed in etched ribbons produced from exfoliated graphene.[6−8] They have no equivalent in any other material than pristine carbon nanotubes[9] and are still not well understood. Transport scenarios involve the topologically protected graphene electronic edge state and multibody interaction in charge-neutral graphene.[3,10] An important question is the sensitivity of the properties to the graphene quality and ribbon edge disorder, as ballistic transport was observed so far only for epigraphene sidewall ribbons, produced directly in shapes at temperatures above 1000 °C and subsequently either annealed in ultrahigh vacuum (UHV) or protected with alumina. Other unconventional electronic transport mechanisms have also been reported in two-dimensional (2D) graphene, such as hydrodynamic flow of the electron fluid even up to relatively high temperatures,[11,12] outlining the rich physics of the system and the need to further investigate these new non-classical electron transport regimes. Such studies should optimally combine local high-resolution electronic measurements and structural studies.

In this Letter, we present high-resolution local resistance measurements as well as 2D maps of the local potential of sidewall epigraphene nanoribbons. Using a scanning probe approach combining atomic force microscopy (AFM) and scanning tunneling microscopy (STM), we both map the potential landscape, as the nanoribbon is voltage-biased along its main axis, and perform local resistance measurements. Most notably, and in contrast with usual STM-based potentiometry mesurements, the technique can be applied to a mixed conducting/insulating surface. The potential (resistance) profile is quasi-independent of distance along extended ribbon segments, indicating larger than μm-long mean-free paths in these quasi-neutral ribbons, even with no high-temperature UHV annealing.

The graphene nanoribbons were epitaxially grown on inclined nanofacets resulting from the annealing of trenches etched in a 4H-SiC substrate[1−3] (see Supporting Information). This technique produces zigzag nanoribbons ~20−100 nm wide on the non-polar $(\bar{1}1215)$ SiC facets with well-defined edge termination.[2,5,13,14] The samples consist of a large number (about a hundred) of mm-long epigraphene nanoribbons connected in parallel. Two extended Ti/Au contacts, about 30 μm apart and perpendicular to the nanoribbons, were evaporated through a SiN stencil mask to avoid organic resists and limit surface contamination. The stencil mask is brought

Received: February 25, 2020
Revised: April 6, 2020
Published: April 9, 2020

https://dx.doi.org/10.1021/acs.nanolett.0c00838
Nano Lett. 2020, 20, 3786–3790

very close to the substrate, as to keep the contact edges sharply defined, with a transition region smaller than 200 nm (see discussion in Supporting Information file). After contact deposition, high-temperature annealing is no longer possible, as it would lead to diffusion of the gold contact on the substrate.

A combined AFM-STM setup[15,16] was operated at room temperature (unless otherwise stated) and under primary (~0.1 mbar) vacuum to measure local resistances (STM probe brought in hard contact with graphene) and the local electrochemical potential (using tunnel contact). In the local resistance method we scan the nanoribbon surface in AFM mode and lower the tip at regular intervals by several nanometers, until a saturation of the tunnel current I_t is reached, at a value I_t^{sat} (see Supporting Information). In agreement with prior reports, the hard contact does not damage the ribbon or the SiC substrate.[3,4] The single tip used here is grounded through the tunnel current preamplifier (Figure 1a). Both gold contacts are brought at *the same*

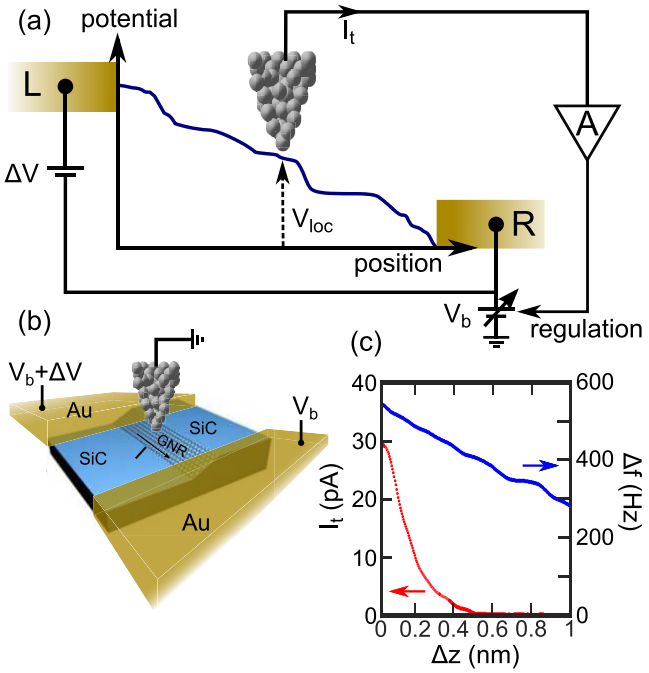

Figure 1. (a) Operating principle of FF-STP. A voltage gradient ΔV from a floating voltage source is applied along a conducting sample confined between two metallic electrodes (L, R). A conducting tip (grounded via the tunneling current preamplifier) is scanned over the sample, and the measurement of the local potential $V_{loc}(x, y)$ is provided by the value of the additional regulation voltage V_b for which $I_t^{dc} = 0$. The tip height regulation is performed simultaneously and independently by FM-AFM regulation. (b) Schematics of the graphene nanoribbon potentiometry experimental setup. (c) Experimental dependence of frequency shift Δf (blue) and tunnel current I_t (red) on the tip−sample distance, measured on a gold thin film (tip oscillation amplitude A = 30 pm, ΔV = 15 mV, V_b = 0).

potential V_b = 10 mV and serve as a counter-electrode. The two-point local resistance between the tip position and the counter-electrodes is defined as $R_{loc} = V_b/I_t^{sat}$. Note that R_{loc} results from two parallel resistances, extending from the tip-nanoribbon contact to either gold contact.

For the local potential measurements, we developed a new scanning potentiometry method that we name force-feedback scanning tunneling potentiometry (FF-STP). It is adapted to the present case of a small conductive wire (or device) on an insulating substrate. High-resolution studies of the surface electrochemical potential are usually performed with STP. The latter is based on STM instrumentation, and the feedback for stabilizing the tip height is provided by the tunnel current or conductance, which restricts measurements to fully conductive surfaces. For insulating substrates, AFM-based potentiometry measurements are frequently used, such as conductive-AFM or electrostatic force microscopy (EFM) and derived techniques.[17,18] However, these AFM-based techniques probe the *electrostatic* rather than the *electrochemical* potential and are far from providing comparable potential and spatial resolution[19] as STM-based techniques.[20−24]

For potentiometry experiments, the combined AFM-STM setup is operated in the non-contact AFM mode using a length extension resonator.[16,25] When operating at very small tip heights, which manifests as a large shift Δf > 100 Hz of the AFM resonator frequency, a tunnel current can flow between the metallic tip and the conductive sample, as seen in Figure 1c. A fixed potential difference ΔV = 15 mV is applied along the sample from a battery, resulting in a position-dependent local potential $|V_{loc}(x, y)| < |\Delta V|$ with respect to the lower potential electrode. To this, an overall sample bias V_b is added, thereby shifting the sample potential as a whole. At a fixed tip position and height, controlled by the AFM signal, a second feedback loop adjusts V_b in order to maintain the dc tunnel current $I_t = (V_{loc} + V_b)/R_t$ at zero (R_t is the tunneling resistance). Note that the ac part of the current, due to the oscillating tip height around its mean value at a frequency of 1 MHz, is beyond the bandwidth of the current amplifier. The non-linear dependence of the current on the oscillating tip height leads to a slight renormalization of the effective tunneling resistance (see discussion in the Supporting Information). At equilibrium, the local potential $V_{loc}(x, y)$ is therefore the opposite of the feedback voltage V_b. This Wheatstone-bridge-type potentiometry method does not require any assumption on the sample or tip local density of states, neither on the tip−sample tunnel resistance, as long as it is not too large (in which case almost no tunneling occurs and the feedback voltage V_b is ill-defined, see Supporting Information). Although the V_b regulation becomes unstable on the non-conductive regions of the sample, the tip-to-sample distance remains the same, as it is independently controlled by the AFM signal. More on the technique can be found in the Supporting Information.

We now move to measurements of the local resistance of individual sidewall ribbons, grown on the mesa shown in Figure 2a,b. Similar to ref 3, scanning tunneling spectroscopy (STS) presented in Figure 2d shows that the ribbon is essentially charge neutral, with a single sharp dI/dV minimum at the Fermi level ±20 meV. This contrasts with STS on the terraces (Figure 2e), where the expected semiconducting density of states of SiC covered by a carbon buffer layer is instead observed, with a marked gap spanning from −500 to +700 meV. Figure 2c shows the local resistance as a function of the curvilinear abscissa s starting from one contact. Several features stand out: a resistance jump of about 40 kΩ, from the first point of measurement on the gold contact to the ribbon, as well as four well-defined flat plateaus over several μm-long segments and transition regions between them. The presence of resistance plateaus and the value of the contact resistance compare well with what was previously observed in similar

https://dx.doi.org/10.1021/acs.nanolett.0c00838
Nano Lett. 2020, 20, 3786−3790

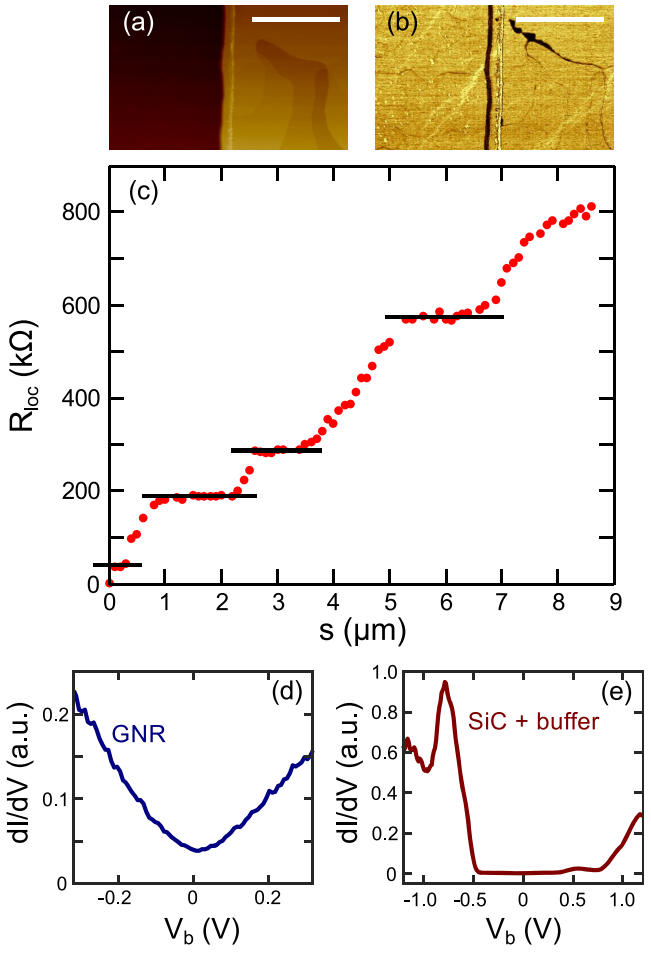

Figure 2. (a) AFM topography image showing the sidewall mesa step and some natural curved SiC steps (height about 1 nm) (scale bar: 1 μm). (b) Lateral force microscopy scan of the same area showing a different friction contrast for graphene grown on the sidewall (black) compared to the terraces. (c) Local contact to ribbon resistance as a function of the curvilinear abscissa s; the gold contact is at s = 0. Several larger that 1 μm-long segments show nearly constant local resistances, with $dR_{loc}/ds \leq 10$ kΩ/μm. (d,e) Low-temperature tunneling spectra on (d) sidewall, displaying a neutral graphene-like density of states, and (e) SiC terraces covered by a carbon buffer-layer, displaying a semiconducting density of state, in agreement with ref 3 (T = 4 K).

zigzag (and curved) sidewall ribbons at charge neutrality, grown both on 4H- and 6H-SiC.[2,3] Note that a recent angle-resolved photoemission spectroscopy study concluded on the absence of flat bands near the Fermi level in the band structure of 4H-SiC zigzag nanoribbons.[26] This non-observation was interpreted as ruling out ballistic transport in the latter, which our findings do not confirm here.

Following the analysis in ref 3, the ribbon resistance at charge neutrality can be written as $R(s) = \alpha(h/e^2)(1 + s/\lambda_0)$, where s is the distance from the contact and λ_0 is the mean-free path. The 40 kΩ contact resistance can be interpreted as a single conductance channel[3] with a transmission α = 0.65. The variation of R_{loc} with distance s on the flat plateaus is below experimental sensitivity. Given the experimental noise, an upper bound of dR_{loc}/ds on the plateaus is ∼10 kΩ/μm, which corresponds to $\lambda_0 > 3.3$ μm. These room-temperature mean path values are remarkably large, all the more given the period of time between ribbon production and the measurement (several months), the exposure to the environment, the contact deposition process, and the absence of postprocessing high-temperature treatment and measurement in non-UHV conditions. These results confirm and expand those found in the extremely well controlled experimental conditions (in UHV or on alumina protected ribbons)[3] and demonstrate the robustness of the ballistic transport in these systems.

In between plateaus, steep dR_{loc}/ds slopes are found, reminiscent of the exponential increase of $R_{loc}(s)$ at large distances, reported in ref 3. Electronic edge state scattering on single-point defects is expected to produce local resistance jumps of the order of h/e^2 at the location of the scattering center,[3,27] which is observed in several instances (see Figure 2c). Elsewhere, seemingly continuous slopes are observed. These might be related to a change in the material itself and the destruction of the conducting edge state at these locations, leading to the large resistivity observed.[5] Alternatively, they could be following the same pattern as the onset of exponential increase of clean ribbons, but on shorter distances. The resurgence of several plateaus is clearly special and worth further investigation.

The local resistance was observed with hard contacts, so we now turn to the non-invasive potential measurements. Figure 3a shows an example of high-resolution local electrochemical potential map of a ∼10 μm-long section of a meandering nanoribbon obtained with a fixed voltage gradient ΔV = 15 mV set between the two gold contacts by a floating voltage source. For better readability, the x-axis scale is strongly compressed compared to the y axis, and the nanoribbon is in reality less meandering than it seems from the map. Even in the case of a very irregular conducting trace, the transverse line cut of Figure 3b shows that the conducting region is confined to the inclined sidewall facet between two SiC(0001) terraces. Outside of the nanoribbon (gray part of the V_b curve), the regulation saturates to a physically irrelevant value a few mV below the local ribbon potential value (see discussion in Supporting Information). Nevertheless, as soon as the tip returns to the conducting regions, the regulation is immediately operative and provides an accurate measure of the local potential $V_{loc} = -V_b$. Note that within the experimental noise level ∼10 μV, the potential is position independent in the transverse direction to the ribbon (see Figure 3c).

The local potential V_{loc} gradually drops along the nanoribbon main axis. However, the potential drop is not monotonous, and extended plateau regions are observed in most measured ribbons where a comparatively flat potential landscape ($dV_{loc}/ds < 100$ μV/μm) is measured over μm-long distances. Figure 3d shows an example of a $V_{loc}(s)$ trace where long plateaus are observed, similar to Figure 2c, despite an irregular topographic structure and the presence of contaminants (see Figures 3d, inset).

Local resistance measurements were also performed on the same nanoribbon segment where the scanning potentiometry was measured. The two experimental quantities can be related *via* elementary circuit equations (the derivation of which is given in the Supporting Information file):

$$V_{calc} = \frac{\Delta V}{2}\left(1 \pm \sqrt{1 - 4\frac{R_{loc}}{R_{tot}}}\right) \quad (1)$$

The calculated local potential can be adjusted to the measured one with a single free parameter that is the total resistance of the nanoribbon R_{tot}. An excellent agreement is

https://dx.doi.org/10.1021/acs.nanolett.0c00838
Nano Lett. 2020, 20, 3786−3790

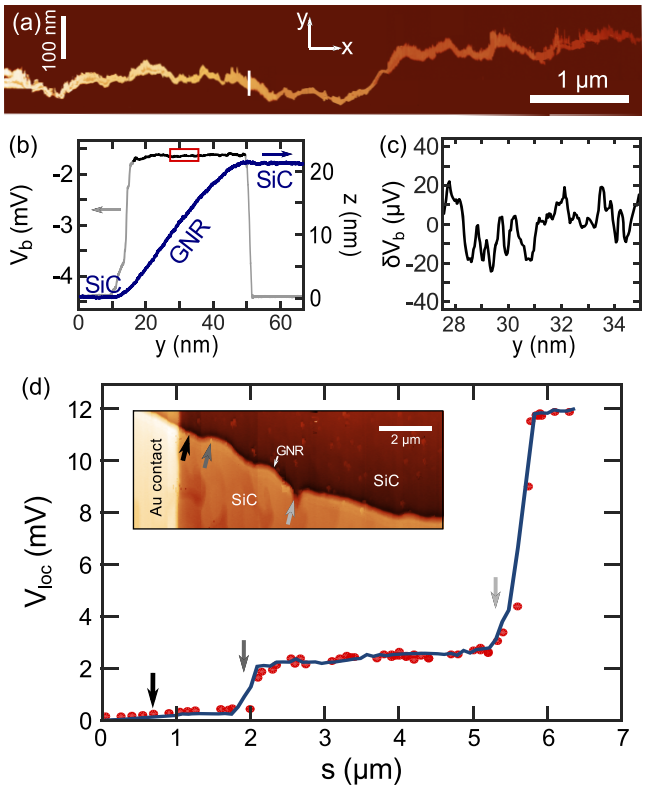

Figure 3. (a) Local potential map of a voltage-biased 40 nm-wide and ~30 μm-long graphene nanoribbon. The overall voltage drop along the nanoribbon segment presented here is about 4 mV. (b) Simultaneously acquired potential and topography profiles in the transverse direction of the nanoribbon. The conductive nanoribbon is on the inclined facet, confined between two insulating buffer-layer-covered SiC terraces. Outside of the inclined facet (gray), the V_b regulation is saturated. (c) Zoomed-in view of the V_b signal, highlighting variations around its local average value. (d) Red dots: Local potential profile measured by FF-STP of another ribbon, averaged over the transverse direction (ΔV = 15 mV and Δf = 300 Hz). The blue line shows the local potential profile calculated from local resistance measurement of the same segment in hard-contact mode, with V_b = 10 mV (see text). (Inset) AFM topography of the measured graphene nanoribbon in the vicinity of a gold contact. Three prominent defects are highlighted by wide arrows. Feedback parameters (with p the respective proportional gains and τ the integration times): V_b feedback: p_V = 8 V/μA, τ_V = 100 μs; frequency modulation AFM: A = 15 pm, Δf = 600 Hz, p_{AFM} = 1 V/μm, τ_{AFM} = 300 μs; height feedback: p_z = 2 pm/Hz, τ_z = 1 ms. The scan speed is 1 nm/s.

found between $V_{loc}(s)$ and $V_{calc}(s)$ (black trace in Figure 3d) with R_{tot} = 72 MΩ (see Supporting Information). It is quite remarkable that despite the overall high ribbon resistance, μm-long segments have a distance dependence of the local potential limited by the experimental resolution. The high ribbon resistance is most probably caused by isolated defects, such as the kink near $s \approx 5.5$ μm (light gray arrow), ribbon irregularities, and adsorbates.

Most importantly, the excellent correlation between the experimental and calculated traces indicates that the local potential as measured by our technique accurately reflects the variations of the local resistance, but without the invasiveness of a hard metal tip pressed against the graphene. Graphene is a textbook case as it is remarkably resistant to hard contact pressure that neither tears graphene nor leaves deposits on it. The equivalence of both potentiometry and resistance techniques for graphene indicates that the local potentiometry method may be used for much more delicate materials, where hard contact would be destructive.

We have looked for structural features at the boundaries of the $V_{loc}(s)$ plateau regions that would signal a change of transport regime. In some cases, such as indicated by the light gray arrow in the inset of Figure 3d, a large topographic disruption of the mesa is observed where the $V_{loc}(s)$ plateau terminates. In other instances, more localized defects (white dot) are seen (black and gray arrows). The $V_{loc}(s)$ plateaus are observed for clean edges (no white dots), yet they appear immune to the sidewall orientation (see for instance between the light and dark gray arrows). Even very irregular ribbons such as the one shown in Figure 3a show longer than μm-long plateaus (6 μm-long plateaus are shown for that ribbon; see Supporting Information).

In conclusion, the quasi distance-independent potential and resistance plateaus observed in epigraphene sidewall nanoribbons confirm larger than μm-long mean-free paths, even though the ribbons were processed with contacts and not measured in UHV. The robustness of the ballistic transport under these conditions, and for meandering ribbons, is remarkable. This is an important step toward large scale use of these ribbons for electronic applications. The new high-resolution potentiometry and local resistance measurements developed here provide consistent information, despite their quite different nature and degree of invasiveness. Applicable to a mixed conducting/insulating surface, the force-feedback technique expands the STP approach to the field of nanoelectronic devices, and, considering its non-invasive character, it can be used to probe high-resolution electrical characteristic of a large variety of materials.

■ ASSOCIATED CONTENT

Supporting Information

The Supporting Information is available free of charge at https://pubs.acs.org/doi/10.1021/acs.nanolett.0c00838.

Description of the FF-STP methods, sample preparation, data on extended plateaus on an irregular ribbon, sample characterization, and ribbon resistance measurements (PDF)

■ AUTHOR INFORMATION

Corresponding Author

Clemens B. Winkelmann − *Université Grenoble Alpes, CNRS, Grenoble INP, Institut Néel, Grenoble 38042, France;* orcid.org/0000-0003-4320-994X; Email: clemens.winkelmann@neel.cnrs.fr

Authors

Alessandro De Cecco − *Université Grenoble Alpes, CNRS, Grenoble INP, Institut Néel, Grenoble 38042, France*

Vladimir S. Prudkovskiy − *Université Grenoble Alpes, CNRS, Grenoble INP, Institut Néel, Grenoble 38042, France; School of Physics, Georgia Institute of Technology, Atlanta, Georgia 30332, United States*

David Wander − *Université Grenoble Alpes, CNRS, Grenoble INP, Institut Néel, Grenoble 38042, France*

Rini Ganguly − *Université Grenoble Alpes, CNRS, Grenoble INP, Institut Néel, Grenoble 38042, France*

https://dx.doi.org/10.1021/acs.nanolett.0c00838
Nano Lett. 2020, 20, 3786−3790

Claire Berger − *Université Grenoble Alpes, CNRS, Grenoble INP, Institut Néel, Grenoble 38042, France; School of Physics, Georgia Institute of Technology, Atlanta, Georgia 30332, United States*

Walt A. de Heer − *School of Physics, Georgia Institute of Technology, Atlanta, Georgia 30332, United States; Tianjin International Center for Nanoparticles and Nanosystems (TICNN), Tianjin University, Tianjin 300072, China*

Hervé Courtois − *Université Grenoble Alpes, CNRS, Grenoble INP, Institut Néel, Grenoble 38042, France*

Complete contact information is available at: https://pubs.acs.org/10.1021/acs.nanolett.0c00838

Notes

The authors declare no competing financial interest.

■ ACKNOWLEDGMENTS

We acknowledge funding from the from the European Union under the Marie Sklodowska-Curie grant agreement 766025, the US AFOSR (FA9550-13-0217), the NSF-ECCS (1506006), and NSF-DMR (1308835). C.B. and V.P. acknowledge funding from the European Union grant agreements 696656 and 785219. This work was also made possible by the French-American Cultural Exchange council through a Partner University Fund and a Thomas Jefferson grant. Dogukan Deniz is warmly thanked for making the sidewall ribbon sample. The devices were processed at the Nanofab platform at Institut Néel with the help of B. Fernandez.

■ REFERENCES

(1) Sprinkle, M.; Ruan, M.; Hu, Y.; Hankinson, J.; Rubio-Roy, M.; Zhang, B.; Wu, X.; Berger, C.; De Heer, W. A. Scalable templated growth of graphene nanoribbons on SiC. *Nat. Nanotechnol.* **2010**, *5*, 727−731.

(2) Ruan, M.; Hu, Y.; Guo, Z.; Dong, R.; Palmer, J.; Hankinson, J.; Berger, C.; De Heer, W. A. Epitaxial graphene on silicon carbide: Introduction to structured graphene. *MRS Bull.* **2012**, *37*, 1138−1147.

(3) Baringhaus, J.; Ruan, M.; Edler, F.; Tejeda, A.; Sicot, M.; Taleb-Ibrahimi, A.; Li, A.-P.; Jiang, Z.; Conrad, E. H.; Berger, C.; Tegenkamp, C.; de Heer, W. A. Exceptional ballistic transport in epitaxial graphene nanoribbons. *Nature* **2014**, *506*, 349−354.

(4) Aprojanz, J.; Power, S. R.; Bampoulis, P.; Roche, S.; Jauho, A.-P.; Zandvliet, H. J.; Zakharov, A. A.; Tegenkamp, C. Ballistic tracks in graphene nanoribbons. *Nat. Commun.* **2018**, *9*, 4426.

(5) Baringhaus, J.; Aprojanz, J.; Wiegand, J.; Laube, D.; Halbauer, M.; Hübner, J.; Oestreich, M.; Tegenkamp, C. Growth and characterization of sidewall graphene nanoribbons. *Appl. Phys. Lett.* **2015**, *106*, 043109.

(6) Han, M. Y.; Brant, J. C.; Kim, P. Electron transport in disordered graphene nanoribbons. *Phys. Rev. Lett.* **2010**, *104*, 056801.

(7) Gallagher, P.; Todd, K.; Goldhaber-Gordon, D. Disorder-induced gap behavior in graphene nanoribbons. *Phys. Rev. B: Condens. Matter Mater. Phys.* **2010**, *81*, 115409.

(8) Dröscher, S.; Knowles, H.; Meir, Y.; Ensslin, K.; Ihn, T. Coulomb gap in graphene nanoribbons. *Phys. Rev. B: Condens. Matter Mater. Phys.* **2011**, *84*, 073405.

(9) Frank, S.; Poncharal, P.; Wang, Z.; De Heer, W. A. Carbon nanotube quantum resistors. *Science* **1998**, *280*, 1744−1746.

(10) Li, J.; Niquet, Y.-M.; Delerue, C. Magnetic-phase dependence of the spin carrier mean free path in graphene nanoribbons. *Phys. Rev. Lett.* **2016**, *116*, 236602.

(11) Crossno, J.; Shi, J. K.; Wang, K.; Liu, X.; Harzheim, A.; Lucas, A.; Sachdev, S.; Kim, P.; Taniguchi, T.; Watanabe, K.; Ohki, T. A.; Chung Fong, K. Observation of the Dirac fluid and the breakdown of the Wiedemann-Franz law in graphene. *Science* **2016**, *351*, 1058−1061.

(12) Bandurin, D.; Torre, I.; Kumar, R. K.; Shalom, M. B.; Tomadin, A.; Principi, A.; Auton, G.; Khestanova, E.; Novoselov, K.; Grigorieva, I.; Ponomarenko, L. A.; Geim, A. K.; Polini, M. Negative local resistance caused by viscous electron backflow in graphene. *Science* **2016**, *351*, 1055−1058.

(13) Palacio, I.; Celis, A.; Nair, M. N.; Gloter, A.; Zobelli, A.; Sicot, M.; Malterre, D.; Nevius, M. S.; de Heer, W. A.; Berger, C.; Conrad, E. H.; Taleb-Ibrahimi, A.; Tejeda, A. Atomic structure of epitaxial graphene sidewall nanoribbons: flat graphene, miniribbons, and the confinement gap. *Nano Lett.* **2015**, *15*, 182−189.

(14) Celis, A.; Nair, M.; Taleb-Ibrahimi, A.; Conrad, E.; Berger, C.; De Heer, W.; Tejeda, A. Graphene nanoribbons: fabrication, properties and devices. *J. Phys. D: Appl. Phys.* **2016**, *49*, 143001.

(15) Senzier, J.; Luo, P. S.; Courtois, H. Combined scanning force microscopy and scanning tunneling spectroscopy of an electronic nanocircuit at very low temperature. *Appl. Phys. Lett.* **2007**, *90*, 043114.

(16) Samaddar, S.; Yudhistira, I.; Adam, S.; Courtois, H.; Winkelmann, C. Charge puddles in graphene near the Dirac point. *Phys. Rev. Lett.* **2016**, *116*, 126804.

(17) Giannazzo, F.; Deretzis, I.; La Magna, A.; Roccaforte, F.; Yakimova, R. Electronic transport at monolayer-bilayer junctions in epitaxial graphene on SiC. *Phys. Rev. B: Condens. Matter Mater. Phys.* **2012**, *86*, 235422.

(18) Panchal, V.; Pearce, R.; Yakimova, R.; Tzalenchuk, A.; Kazakova, O. Standardization of surface potential measurements of graphene domains. *Sci. Rep.* **2013**, *3*, 2597.

(19) Woodside, M. T.; McEuen, P. L. Scanned probe imaging of single-electron charge states in nanotube quantum dots. *Science* **2002**, *296*, 1098−1101.

(20) Willke, P.; Druga, T.; Ulbrich, R. G.; Schneider, M. A.; Wenderoth, M. Spatial extent of a Landauer residual-resistivity dipole in graphene quantified by scanning tunnelling potentiometry. *Nat. Commun.* **2015**, *6*, 6399.

(21) Wang, W.; Munakata, K.; Rozler, M.; Beasley, M. R. Local transport measurements at mesoscopic length scales using scanning tunneling potentiometry. *Phys. Rev. Lett.* **2013**, *110*, 236802.

(22) Xie, T.; Dreyer, M.; Bowen, D.; Hinkel, D.; Butera, R.; Krafft, C.; Mayergoyz, I. A scanning tunneling microscopy based potentiometry technique and its application to the local sensing of the spin Hall effect. *AIP Adv.* **2017**, *7*, 125205.

(23) Yoshimoto, S.; Murata, Y.; Kubo, K.; Tomita, K.; Motoyoshi, K.; Kimura, T.; Okino, H.; Hobara, R.; Matsuda, I.; Honda, S.-i.; Katayama, M.; Hasegawa, S. Four-point probe resistance measurements using PtIr-coated carbon nanotube tips. *Nano Lett.* **2007**, *7*, 956−959.

(24) Bannani, A.; Bobisch, C.; Möller, R. Local potentiometry using a multiprobe scanning tunneling microscope. *Rev. Sci. Instrum.* **2008**, *79*, 083704.

(25) Samaddar, S.; Coraux, J.; Martin, S. C.; Grévin, B.; Courtois, H.; Winkelmann, C. B. Equal variations of the Fermi level and work function in graphene at the nanoscale. *Nanoscale* **2016**, *8*, 15162−15166.

(26) Miettinen, A. L.; Nevius, M. S.; Ko, W.; Kolmer, M.; Li, A.-P.; Nair, M. N.; Kierren, B.; Moreau, L.; Conrad, E. H.; Tejeda, A. Edge states and ballistic transport in zigzag graphene ribbons: The role of SiC polytypes. *Phys. Rev. B: Condens. Matter Mater. Phys.* **2019**, *100*, 045425.

(27) Datta, S. *Electronic transport in mesoscopic systems*; Cambridge University Press: Cambridge, UK, 1997.